JOURNAL OF APPLIED ELECTROCHEMISTRY **26** (1996) 1083–1092

Anodic dissolution of nickel in concentrated sulfuric acidic solutions

G. CORDEIRO, O. R. MATTOS

Lab. de Corrosão "Prof. Manoel de Castro", EE/PEMM/COPPE/UFRJ, Brazil

O. E. BARCIA

Departmento Fisico-Química, IQ/UFRJ, Brazil

L. BEAUNIER, C. DESLOUIS, B. TRIBOLLET

UPR 15 du CNRS, Laboratoire Physique des Liquides et Electrochimie, Paris, France

Received 14 August 1995; revised 4 March 1996

The anodic dissolution of nickel in concentrated sulfuric acidic solutions is characterized by two diffusion plateaux related to the active and transpassive regions. For the same speed of rotation of a rotating disc electrode, the two plateaux currents are almost identical. However, the less anodic one gives rise to a rough electrode surface while a polished surface is observed at the more anodic one. For nickel as-received, mass transport influences the current over the whole potential range. After heat treatment, only the current for the two plateaux were mass transport controlled. Electrochemical impedance diagrams show that the lowest frequency capacitive loop is influenced by mass transport. Electrohydrodynamic (EHD) impedance diagrams show two different regions. In the low frequency range, the results follow the theoretical curve corresponding to a uniformly accessible electrode with a very high Schmidt number around 10^7. At high frequency, the EHD impedance may correspond to an interface covered by a gel layer formed from the products of the anodic dissolution.

1. Introduction

The electropolishing of metals is a common surface treatment process [1] but its mechanism is not yet well understood in the case of nickel. Nickel in concentrated H_2SO_4 can be actually electrochemically polished at high anodic overpotentials. This system has been studied at steady state (polarization curves) as a function of the sulfate concentration [2, 3]. In general, the curves present two current maxima: the first maximum defines the activation/passivation transition and the second defines the transpassive dissolution/secondary passivation transition. For an H_2SO_4 concentration higher than 10 M, two plateaux are observed in the polarization curves, instead of two maxima. It is noteworthy that the currents have practically the same value, despite the fact that the surface aspect in each plateau is not similar: in the activation plateau a generalized attack occurs, whereas in the transpassivation one, the surface is electropolished.

Hoar *et al.* [2, 4, 5] assumed that electropolishing occurs through a film at the electrode surface. This film acts as a cation acceptor which removes the metallic ions from the surface to achieve electropolishing. A similar hypothesis was assumed by Keddam *et al.* [3] from optical microscopy observations of the electrode surface. They proposed that for concentrations greater than 10 M only, the anodic film is sufficiently compact and adherent, allowing the electropolishing of the electrode. The authors found that the limiting current, I_L, followed a Koutecky–Levich equation, that is $I_L^{-1} = A + B\Omega^{-1/2}$, where Ω is the steady rotation speed of electrode. In this equation A^{-1} represents the maximum mass transport rate through the film ($\Omega \rightarrow \infty$). For the activation plateau, the authors observed $A = 0$.

In this paper, the kinetics of nickel electropolishing at high H_2SO_4 concentration is studied by polarization curves, electrochemical and EHD impedances. The EHD impedance is a technique based on frequency analysis of the current (potentiostatic case) or potential (galvanostatic case) in response to a sinusoidal speed modulation for a rotating disc electrode [6]. This technique is an appropriate method for measuring Schmidt number (*Sc*) without having to know the concentration of electroactive species. From the Schmidt number, *Sc*, which is the ratio of the solution kinematic viscosity to the diffusivity of the reacting or produced species, the latter quantity can be determined. EHD impedance allows accurate distinction of a uniformly accessible surface from a partially blocked one [6]. Moreover, by this technique, it is also possible to characterize a surface coated with a porous film [6], when mass transport inside the film becomes rate determining.

This paper deals essentially with an experimental

0021-891X

study in which the influence of several parameters is examined in view of a future modelling.

2. Experimental details

The working electrode used was a cylindrical rod (0.2 cm^2) of nickel (Johnson-Matthey). The rod specimens were embedded in an epoxy resin mould with only their cross section allowed to contact the electrolyte and shaped as a rotating disc electrode. The electrode was used as-received and heat-treated for 48 h at 900 °C. Figure 1 shows the scanning electron microscope (SEM) photographs after polarization on the activation plateau for the metal as-received (Fig. 1(a)) and for the heat-treated metal (Fig. 1(b)). The heat treatment was made with a view to increasing the grain size and also decreasing the defects in the crystalline structure. A (1 1 1) single crystal of nickel was also used. The reference electrode was a saturated sulfate electrode (SSE) and the counter electrode was a cylindrical platinum grid of large area.

The solutions were prepared with H_2SO_4 (Merck) and double-distilled water. The cell was placed in a constant temperature bath which was controlled and maintained at 25.0 ± 0.5 °C or 5.0 ± 0.5 °C.

The current–potential curves were recorded in potentiostatic mode by means of a potentiostat (Omnimetra Instruments) and a plotter (Hewlett-Packard 7090A X–Y Recorder). Electrochemical and EHD impedance measurements were performed with a Solartron 1250 frequency response analyser (FRA).

3. Results

3.1. *Steady-state results*

Figure 2 shows the polarization curves for sulfuric acid (12 M) as a function of the electrode rotation speed. Two electrolyte temperatures were imposed: 25 °C (Fig. 2(a)) and 5 °C (Fig. 2(b)). As already known for 25 °C [3], two plateaux are also obtained at 5 °C. The presence of these plateaux indicates precipitation of salts which may be of different nature for each plateau. The precipitation of salts, can induce two physical situations: (i) a porous film layer and (ii) a precipitated salt which forms a colloidal dispersion within the solution and close to the metal surface [7].

In Fig. 3, Koutecky–Levich plots (I_L^{-1} against $\Omega^{-1/2}$) for the activation and transpassivation plateaux are given. At 25 °C and 5 °C, the current for the activation plateau follows the relation $I_L^{-1} = B\Omega^{-1/2}$ whereas for the transpassivation one $I_L^{-1} = A + B\Omega^{-1/2}$. These results show that the

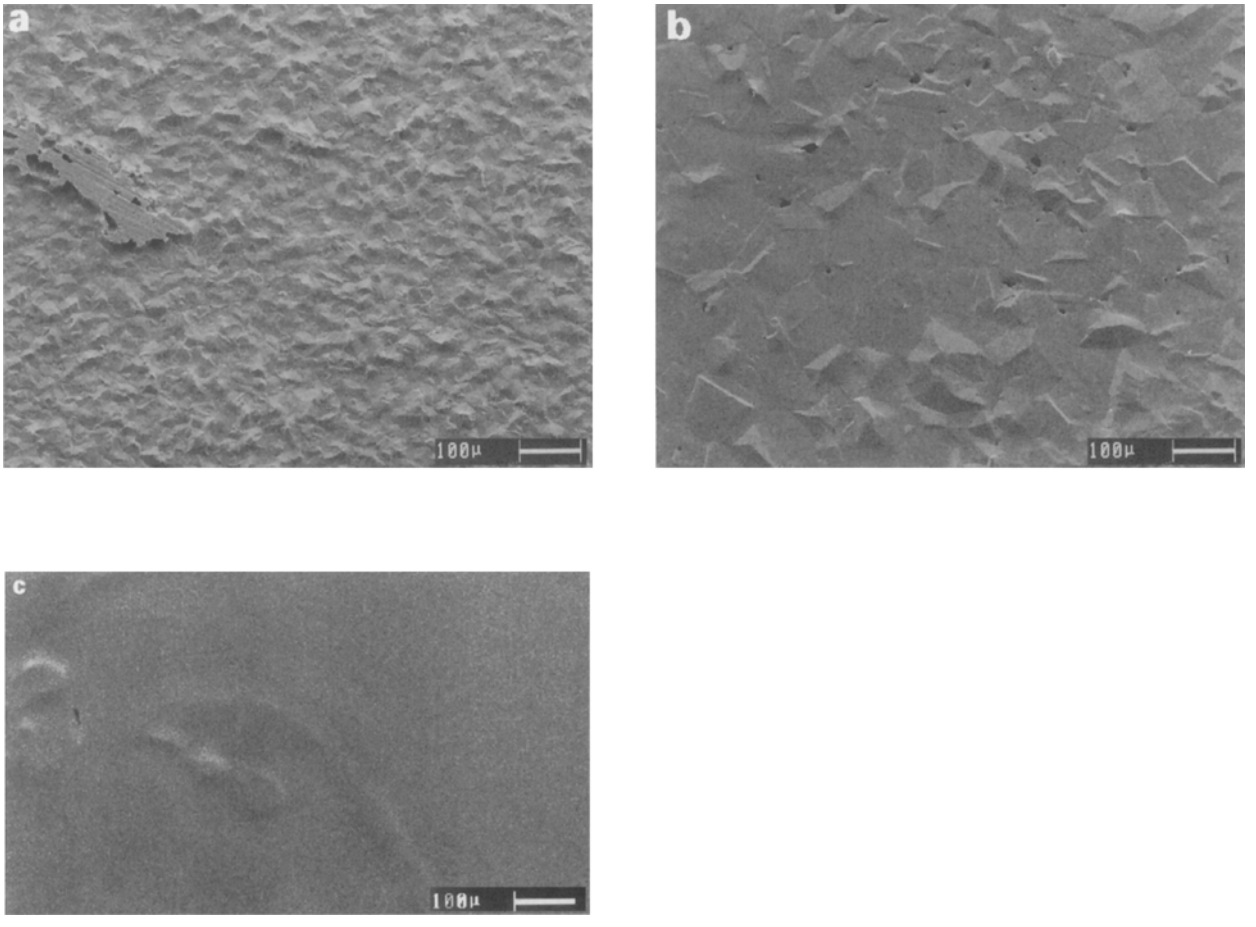

Fig. 1. SEM photographs showing the nickel surface after polarization at the activation plateau in H_2SO_4 (24 N): (a) without heat treatment; (b) with heat treatment or (c) at the transpassivation plateau.

electrode surface during the transpassivation process is covered by a film or is partially blocked [8, 9]. The activation plateau may represent a surface without film or with a film with thickness varying as $\Omega^{1/2}$ [10].

Despite the similarity of the steady behaviour for both plateaux, the visual aspect of the electrode surface is not the same in these two conditions. Indeed, at the activation plateau, a generalized attack is observed and the grains are revealed (Fig. 1(a) or (b)). At the transpassivation plateau, an electropolishing process occurs and the micro roughness disappears (Fig. 1(c)). The above visual characteristic is found for 25 °C and 5 °C.

In Fig. 4(a) and (b) the polarization curves for nickel are compared as-received (a) and after heat treatment (b). The value of the current for both plateaux is nearly the same. However, the activation plateau is better defined in Fig. 4(a); the transpassive dissolution (i.e., between 0.5 and 1 V vs SSE) is slightly influenced by mass transport in Fig. 4(b) and the transpassivation plateau is not influenced by the heat treatment. In Fig. 4(c) the polarization curves are presented for a single crystal of nickel. The activation plateau is reduced to a peak. The transpassivation plateau is partly mass transport controlled, with a finite slope (equal to the reciprocal of the polarization resistance R_p). Moreover, the transpassive dissolution (i.e., between 0.5 and 1 V vs SSE) is qualitatively the same as compared to the heat-treated nickel, where the current is quite independent of mass transport. This suggest that the layers existing at the activation plateau depend on the microstructure of the electrode and, to a lower degree, for the transpassivation plateau. Moreover, the heat-treated nickel, and also the single crystal nickel show that transpassive dissolution is only controlled by charge transfer with practically no mass transport influence.

In Fig. 5, the influence of H_2SO_4 concentration on the polarization curves is presented, for 5 °C. The current is constant between the activation and the passivation plateaux but only the transpassivation range of the curves is given. For 12 and 13 M sulfate, a plateau is clearly detected and electropolishing occurs. For higher concentrations, a generalized attack takes place and no influence of mass transport at the activation and transpassivation plateaux is observed. These results show that a minimum concentration of free water is necessary to achieve electropolishing. Therefore water needs to be taken into account in the film structure at the transpassivation plateau and this feature must be considered in the dissolution kinetics.

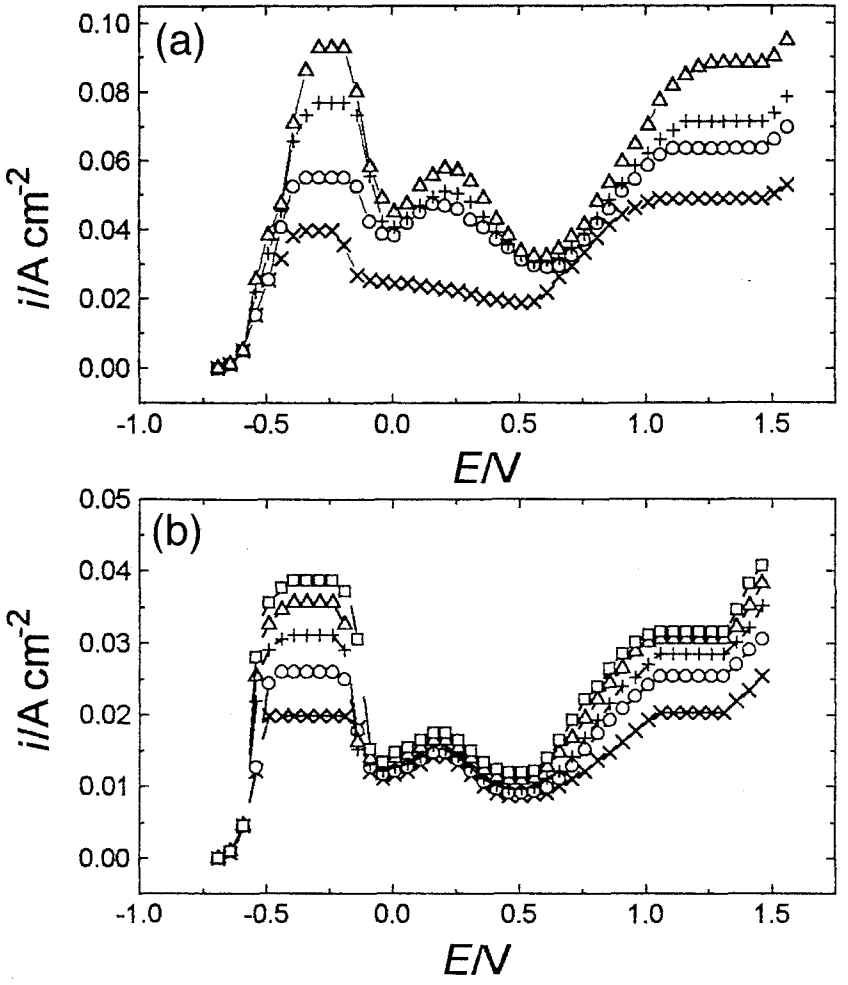

Fig. 2. Polarization curves obtained for nickel in H_2SO_4 (24 N). (a) 25 °C; (b) 5 °C. Rotation rate: (×) 120, (○) 240, (+) 360, (△) 480 and (□) 600 rpm.

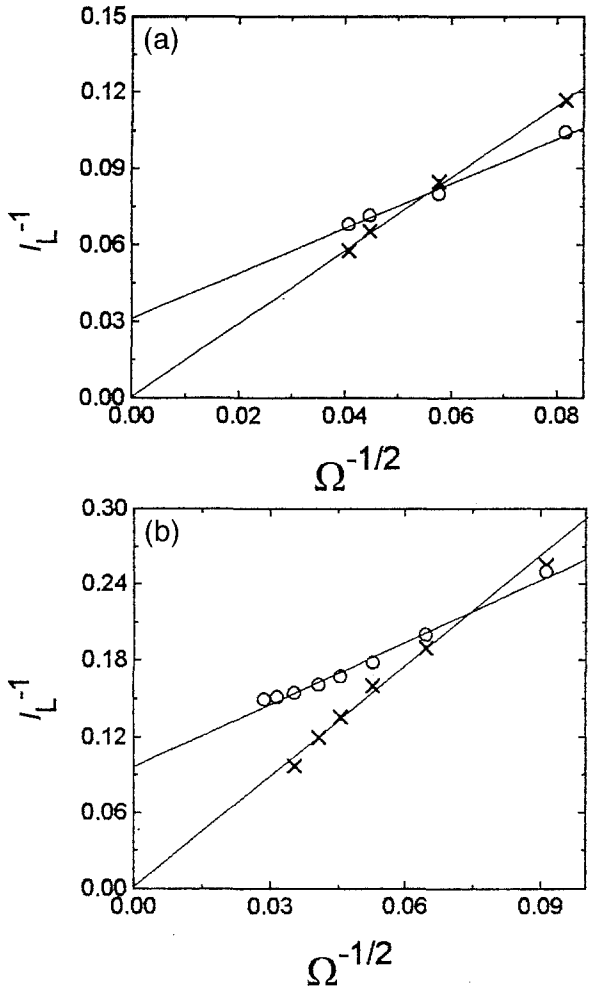

Fig. 3. Koutecky–Levich plots obtained for nickel in H_2SO_4 (24 N). (a) 25 °C; (b) 5 °C. -activation (−0.35 V); -transpassivation (1.2 V).

3.2. *Electrochemical and EHD impedances results*

In the following, the EHD and the electrochemical impedances concerning the transpassivation plateau obtained for H_2SO_4 (12 M) at 5 °C are presented. All diagrams were taken at 1.2 V vs SSE.

3.2.1. EHD impedance. Figure 6 shows the diagrams for nickel as-received. The normalized amplitudes fall on the same curve for dimensionless frequency $p < 0.3$, p being the ratio of the modulation frequency $\omega/2\pi$ to the mean RDE rotation frequency $\Omega/2\pi$. For $p > 0.3$, the curves are separated at different Ω values. In contrast, the phase shift data fall on a single curve for all p values and a limit around 450° is obtained. This Figure also shows the curve for a Schmidt number of 10^7, based on the predictions of Tribollet and Newman for a uniformly accessible electrode [11].

The EHD impedance for the heat-treated electrode is shown in Fig. 7. The curves present the same qualitative behaviour as that obtained in Fig. 6. For this electrode, Fig. 8 shows the EHD impedance against frequency in hertz instead of the dimensionless frequency p. In the high frequency range, the amplitude data merge onto a single curve for all rotation speeds. Figure 9 presents the EHD impedance for the single crystal. For $p < 1$ the curves show similar results to those already seen in the previous Figures. The particular point here concerns the region of high frequencies, $p > 1$. In this region, $A(p)/A(0) < 10^{-3}$, the experimental points are very scattered and a limiting phase shift is hardly seen. For this electrode it was not possible to analyse the high frequency region.

3.2.2. Electrochemical impedance. Figures 10–12 show the electrochemical impedance diagrams obtained for nickel as-received, heat-treated and single crystal, respectively. For the first two conditions described above, Figs 10 and 11, the diagrams are very similar. Five loops are observed: one high frequency loop associated with the double layer, followed by an inductive loop around 1 Hz; a capacitive loop around 0.7 Hz; another inductive loop around 0.12 Hz, only clearly seen at low rotation speeds, and finally one capacitive loop around 0.02 Hz. In Fig. 12, only four loops are detected: the lowest frequency capacitive loop seen in the previous figures is no longer observed and the process at lower frequencies is an inductive loop around 0.1–0.2 Hz. The capacitive loop at the lowest frequency, seen in Figs 10 and 11, seems to be related to the mass transport process because its diameter is an inverse function of the disc rotation speed and the characteristic frequency of this loop is the same as the frequency seen in the EHD impedance at 90° (Fig. 6). The inductive loop in these figures around 0.1 Hz is related to the charge transfer process occurring during electropolishing. Indeed, this loop is not influenced by the rotation speed and is better seen for the single crystal, where the current is no longer only mass transport controlled. It is important to note in the previous diagrams that the limit for $\omega \to 0$, Rp^{-1}, is consistent with dI/dE of the steady polarization curves only in the case of the single crystal, where a finite Rp is observed. For the other working electrodes (nickel as-received and heat-treated), the diagrams show a finite limit while Rp from the steady polarization curves is infinite. This point is not explained in this paper and the cause is not yet well understood.

4. Discussion

As shown above, the concentration of free water seems to be a crucial parameter for analysing the experimental results. This can be emphasized by plotting the transpassivation plateau current value as function of the total water content (though activity should be preferred for those high acidic concentrations) as displayed in Fig. 13. It can be seen that there is first a linear domain represented by a dashed line corresponding to the higher acidic concentrations with an extrapolated limit at about 1.5 mA for zero water content. For higher water contents, the current increase is much faster, the transition corresponding to a concentration of about 14 M. This transition

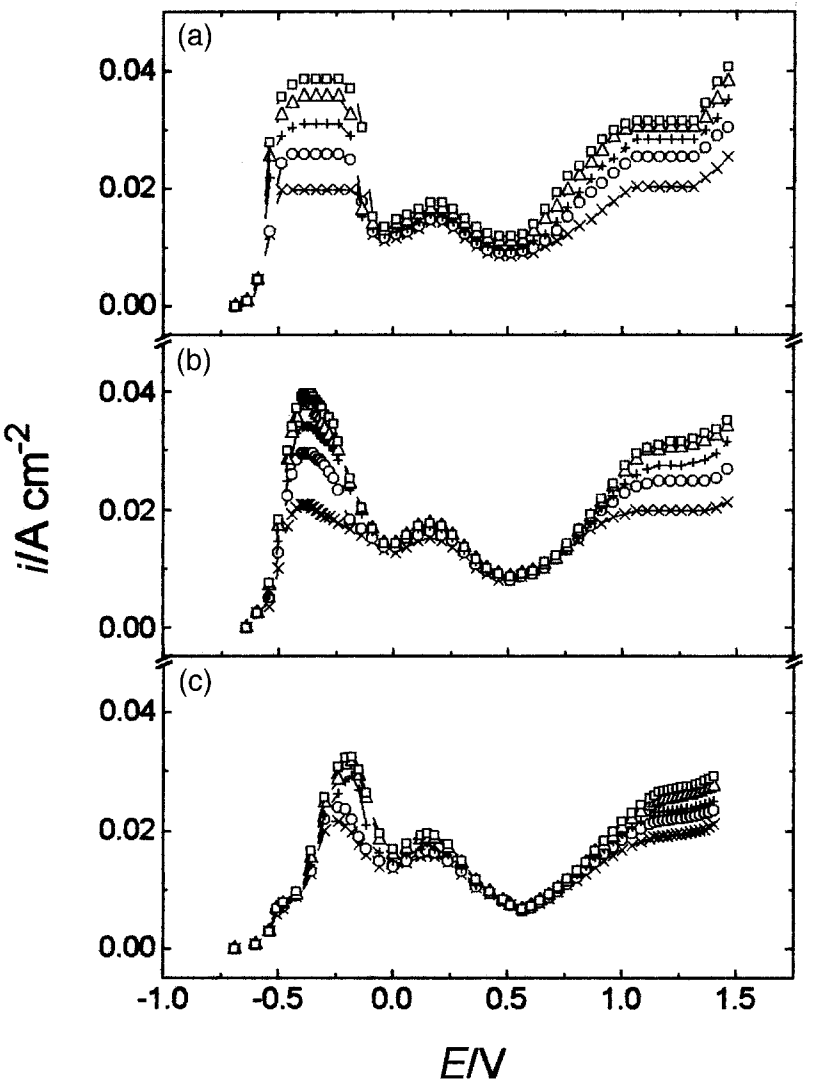

Fig. 4. Polarization curves obtained for nickel in H_2SO_4 (24 N). (a) Without heat treatment; (b) with heat treatment; (c) (1 1 1) single crystal. Rotation rates: (×) 120, (○) 240, (+) 360, (△) 480 and (□) 600 rpm.

seems to mark a change in the nature and properties of the external layer. Above this water content, the current is mass transport controlled and not for the low water contents. Also, as observed by Keddam *et al.* [3], in the low water content regime, the interface seems to be covered with a compact layer. In addition, this latter regime is characterized, at the transpassivation plateau, by the disappearance of electropolishing and a generalized attack occurring, as for the dissolution plateau.

On the basis of these results, for steady, electrochemical and EHD impedances, the following can

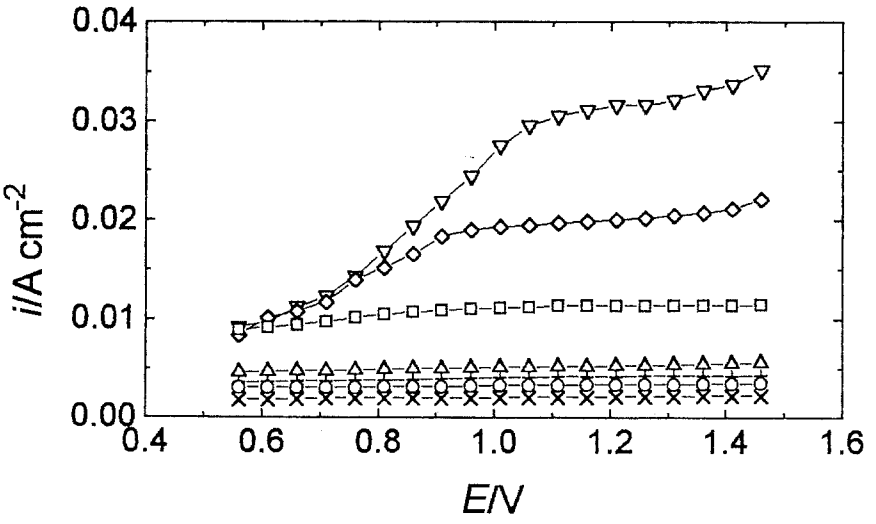

Fig. 5. Polarization curves obtained for nickel in different H_2SO_4 concentrations: (×) 36, (○) 34, (+) 32, (△) 30, (□) 28, (◇) 26 and (▽) 24 N.

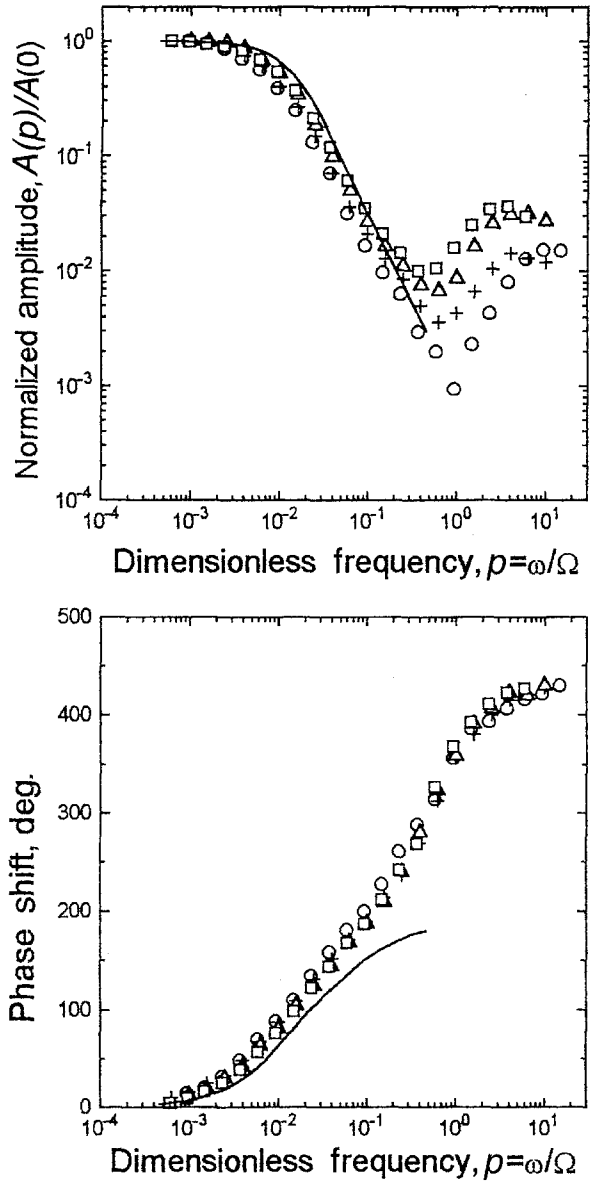

Fig. 6. EHD impedance diagrams obtained for nickel (without heat treatment) in H_2SO_4 (24 N). $Sc = 10^7$. Rotation rates: (○) 240, (+) 360, (△) 480 and (□) 600 rpm.

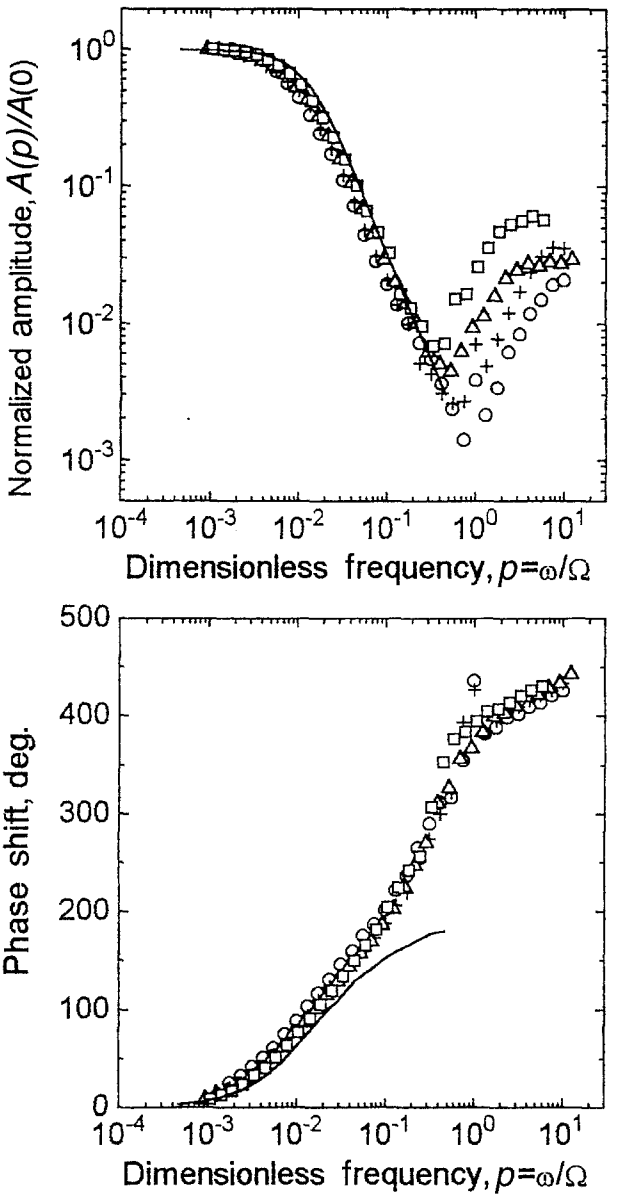

Fig. 7. EHD impedance diagrams obtained for nickel (with heat treatment) in H_2SO_4 (24 N). Rotation rates: (○) 240, (+) 360, (△) 480 and (□) 600 rpm.

be stated. For all covered conditions in potential and rotation speed, the existence of two superposed layers can be postulated. The first and inner one is due to oxide formation. The maximum current which can flow through this layer is defined by a high field assisted transport [12] and is the non-diffusional current A appearing in the Koutecky–Levich relations. In other words, the A term corresponds to a kinetic limitation by this high field conduction process and would give the value of the current in the absence of mass transport limitation (i.e., for an infinite rotation speed). This means that the oxide formed at the dissolution plateau is not the rate determining step. At the transpassivation plateau, this component becomes measurable which means either that the oxide changes in nature or that its thickness and compactness increase.

However, in both situations, the control is mainly due to mass transport in the second and outer hydrated sulfate layer which is identical on the two plateaux as shown by the EHD impedance diagrams. For the higher water contents, that is, in so far as the current is controlled by hydrodynamics, this nickel sulfate contains seven water molecules according to the observations made at lower acidic concentrations [3]. For the lower water contents, the nature of the nickel sulfate seems to change and a lower degree of hydration (monohydrate) can be hypothesized. The current then becomes migration-diffusion controlled and the decrease observed when the acidic concentration increases is due to the fact that less free water is available for ions solvation; this means that the critical concentration at the oxide/salt interface of all involved ionic or neutral species decrease because their apparent concentration becomes smaller.

The EHD impedances obtained for different rotation speeds fall onto a single curve for 0.3. This behaviour is characteristic of a uniformly accessible surface, but the measured Schmidt number is around

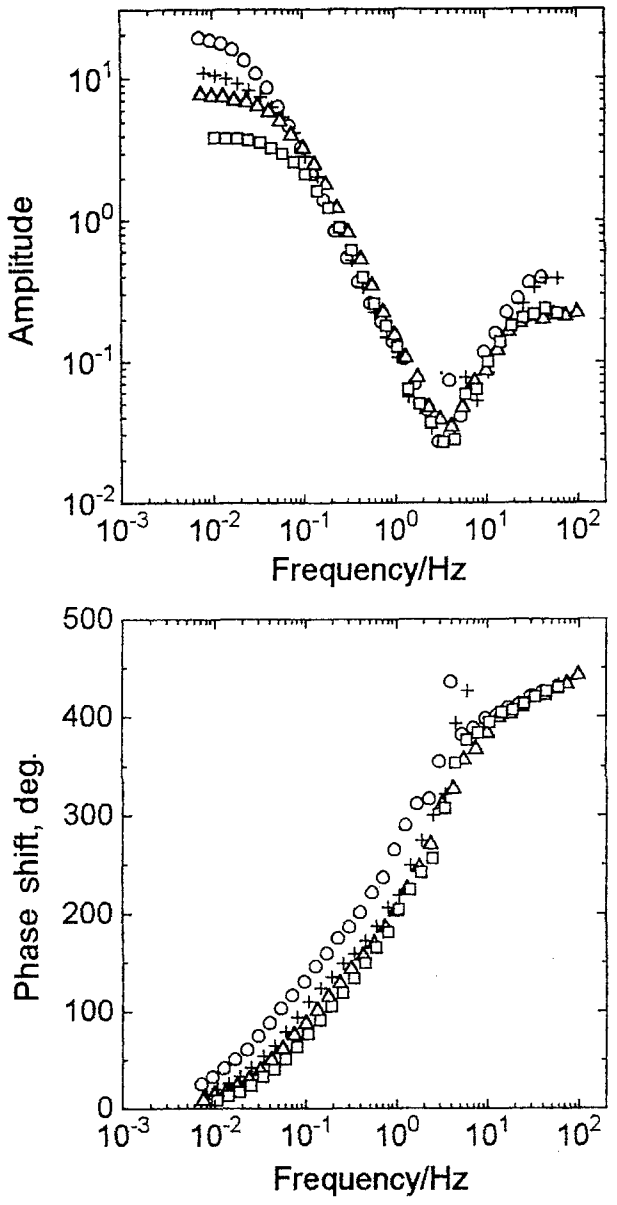

Fig. 8. EHD impeadance diagrams, as a function of frequency/2, obtained for nickel (with heat treatment) in H_2SO_4 (24 N), Rotation rates: (○) 240, (+) 360, (△) 480 and (□) 600 rpm.

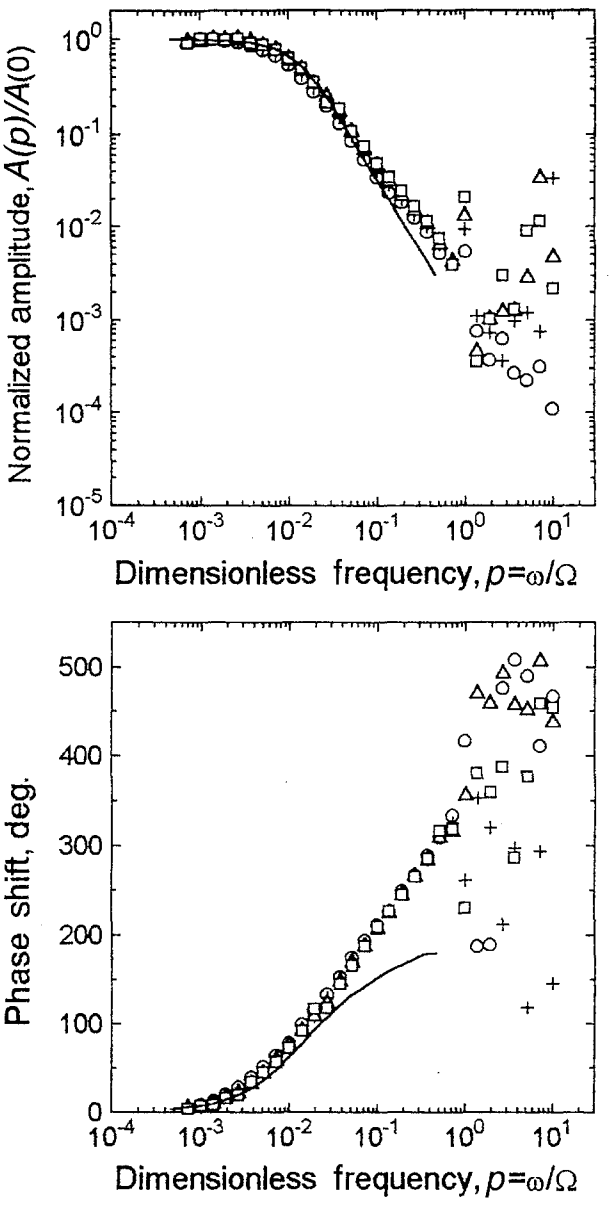

Fig. 9. EHD impedance diagrams obtained for a nickel single crystal in H_2SO_4 (24 N). $Sc = 10^7$. Rotation rates: (○) 240, (+) 360, (△) 480 and (□) 600 rpm.

10^7. Such a high Schmidt number value is not usual for a liquid and is much higher than the value based on the bulk quantities for both the solution viscosity and the diffusivity of the neutral or ionic species which are responsible for the rate determining step by mass transport. For similar conditions of electropolishing of copper in phosphoric acid, such high *Sc* values were obtained using the EHD impedance technique, and were ascribed to water as diffusing species in the frame of a water acceptor model [13–15]. As a matter of fact, in most of the dissolution models proposed so far for nickel (not detailed here), water is not consumed in the electrochemical steps. In contrast, water is consumed during the formation/dissolution of the sulfate layer and its transport can be hence assumed to be the rate determining step. But this layer must be loosely structured because, as mentioned above, its behaviour is rather that of a viscous liquid [8]. Therefore, a two phase layer formed by a concentrated suspension of sulfate crystallites can provide a realistic description.

The second characteristic feature of the EHD diagrams is the prevailing influence at high frequencies of a term varying as $-j\omega$ (indicated by a limiting phase shift of $-450° = -360° - 90°$ and by an amplitude increasing proportionally to frequency $\omega/2\pi$). It is also worth mentioning that a response at the same characteristic frequency (around 10 Hz) is not detected in the a.c. impedance diagrams. This process is therefore not associated to mass transfer in the liquid, induced by the flow modulation but is the result of a direct mechanical effect by the shear stress modulation of the flow at the interface.

Considering this behaviour, one may postulate that this two-phase outer layer has a gel-like structure which behaves as a viscoelastic medium at high frequencies. In fact, such a high frequency behaviour was previously explained as due to elastic properties

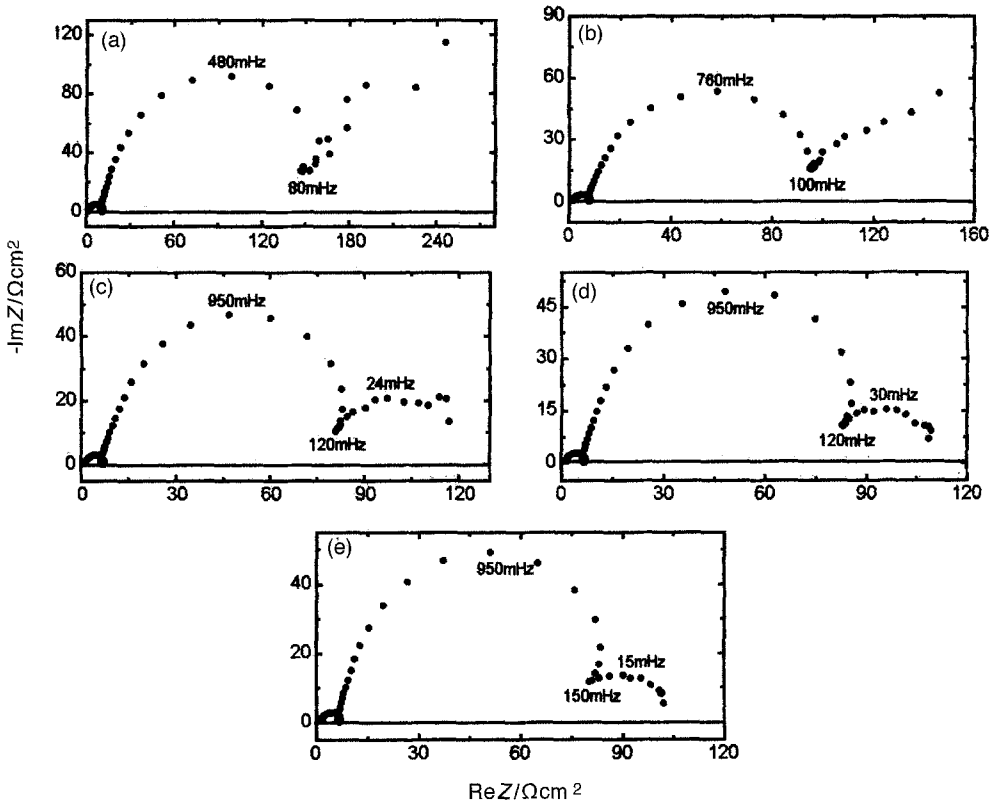

Fig. 10. Electrochemical impedance diagrams obtained for nickel (without heat treatment) in H_2SO_4 (24 N): (a) 120 rpm, (b) 240 rpm, (c) 360 rpm, (d) 480 rpm and (e) 600 rpm.

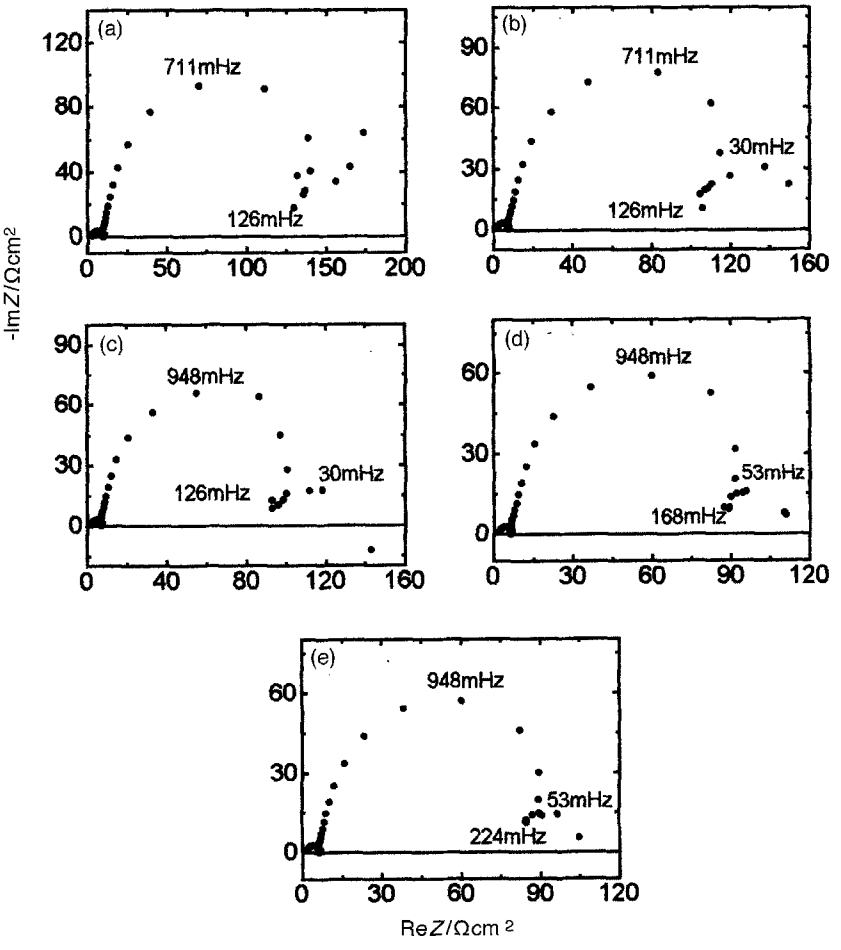

Fig. 11. Electrochemical impedance diagrams obtained for nickel (with heat treatment) in H_2SO_4 (24 N): (a) 120 rpm, (b) 240 rpm, (c) 360 rpm, (d) 480 rpm, and (e) 600 rpm.

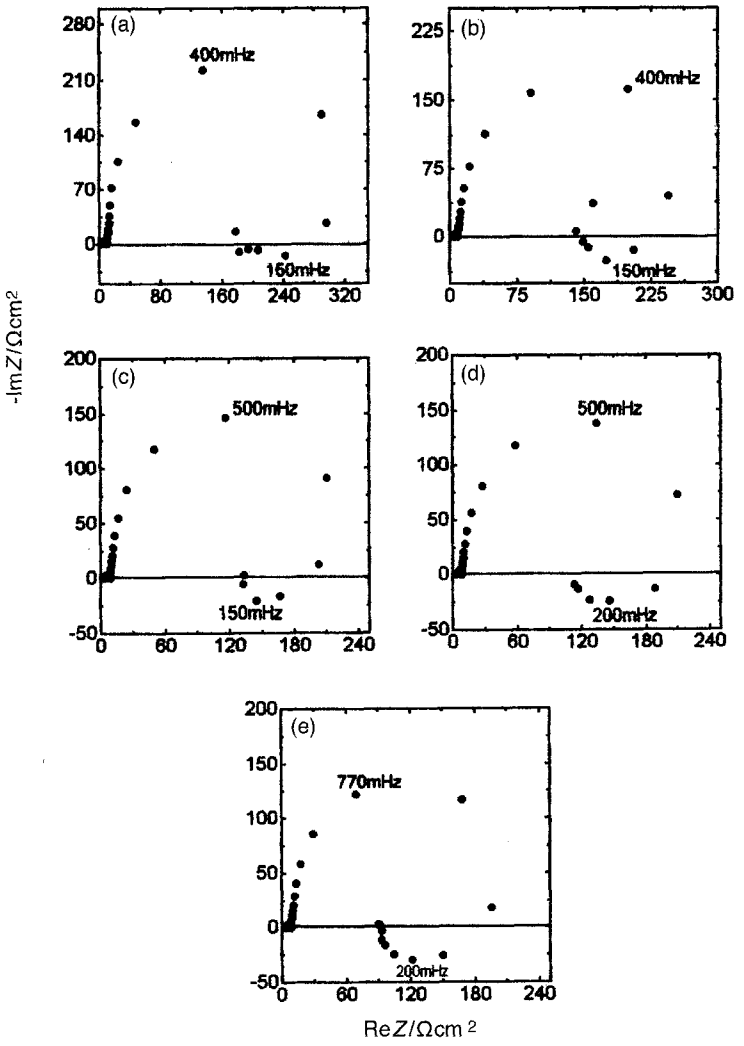

Fig. 12. Electrochemical impedance diagrams obtained for a nickel single cyristal in (24 N) H_2SO_4 solution: (a) 120 rpm, (b) 240 rpm, (c) 360 rpm, (d) 480 rpm and (e) 600 rpm.

of a layer with modulation of the associated capacitance by modulation of its thickness [16]. In steady-state, this capacitance has no effect. When the shear is modulated this modulates the film thickness and hence its capacitance which gives an additional modulated current. This layer, which has a low free water content, and hence a small dielectric constant, and a thickness higher than a usual double layer, corresponds to a low capacitance value.

At higher acid concentrations (low water contents) the nature of this outer layer probably changes, which explains that the same features as on the dissolution plateau are observed. This also modifies the underlying oxide layer which does not change between the activation and transpassivation conditions, the salt layer bearing the whole potential drop.

4. Conclusion

The electrochemical processes occurring at the two plateaux of the polarization curves of nickel in high H_2SO_4 concentration are not the same. The transpassivation plateau is characterized by the electropolishing of the electrode, whereas the activation one is associated with a generalized attack.

Concerning the transpassivation plateau, the following points may be made: (i) water is necessary and needs to be taken into account in the film structure; (ii) a very high Schmidt number is associated with it; (iii) a relation $I_L^{-1} = A + B\Omega^{-1/2}$ represents its kinetic behaviour; (iv) the EHD impedance diagrams present two distinct ranges: at low frequency there is a single curve for all rotation speeds whereas at high frequency there are separate diagrams. However, when the EHD impedance plots are given as function of absolute frequency (in hertz), the amplitude diagrams show a single curve for all rotation speeds at high frequency; and, finally, (v) the electrochemical impedance shows a capacitive loop at the lowest frequency controlled by mass transport.

Taking into account the above features, a duplex structure of the film composed of a thin oxide layer at the electrode surface covered by a gel film is postulated.

Acknowledgements

This work is a part of the CAPES/COFECUB research program 115/90/95. The Brazilian authors thank the CNPq, Finep and CAPES.

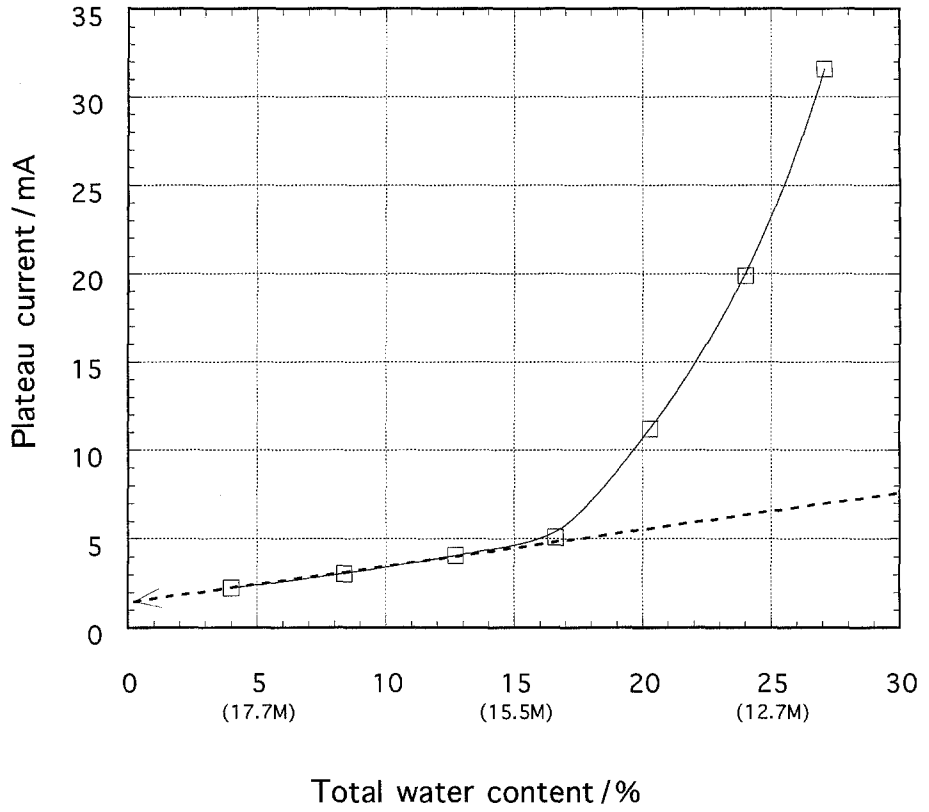

Fig. 13. Limiting current at the transpassivation plateau as function of the total water content (%). The values between parentheses on the abscissae represent the acidic molarity.

References

[1] P. A. Jacquet, *Trans. Electrochem. Soc.* **69** (1938) 629.
[2] G. P. Rothwell and T. P. Hoar, *Electrochim. Acta* **10** (1965) 403.
[3] M. Daguenet, M. Froment, and M. Keddam, *J. Microscopie* **5** (1966) 569.
[4] T. P. Hoar and G. P. Rothwell, *Electrochim. Acta* **9** (1964) 135.
[5] T. P. Hoar, D. C. Mears and G. P. Rothwell, *Corros. Sci.* **5** (1965) 279.
[6] C. Deslouis and B. Tribollet, *in* 'Advances in Electrochemical Science and Engineering' (edited by Gerisher and Tobias), vol. 2 (1991), p. 205.
[7] O. E. Barcia, O. R. Mattos and B. Tribollet, *J. Electrochem. Soc.* **139** (1992) 446.
[8] C. Deslouis, B. Tribollet, M. Duprat and F. J. Moran, *ibid.* **134** (1987) 2496.
[9] A. Caprani, C. Deslouis, S. Robin, and B. Tribollet, *J. Electroanal. Chem.* **238** (1987) 67.
[10] O. E. Barcia, O. R. Mattos, N. Pebere and B. Tribollet, *J. Electrochem. Soc.* **140** (1993) 2825.
[11] B. Tribollet and J. Newman, *ibid.* **130** (1983) 2016.
[12] K. Arnold and K. J. Vetter, *Z. Elektrochem.* **64** (1960) 407.
[13] R. Vidal and A. C. West, *J. Electrochem. Soc.* **142** (1995) 2682 and 2689.
[14] S. H. Glarum and J. H. Marshall, *ibid.* **132** (1985) 2872.
[15] M. Matlosz, *Electrochimica Acta* **40**(4) (1995) 393.
[16] C. Deslouis, M. C. Lafont, N. Pebere and D. You, *Corros. Sci.* **34** (1993) 1567.